JAERI-M
93-224

SIMULATION OF TEARING MODE STABILIZATION BY USING ECH

November 1993

Gen-ichi KURITA, Takashi TUDA
Masafumi AZUMI and Tatsuoki TAKEDA

日本原子力研究所
Japan Atomic Energy Research Institute

JAERI-Mレポートは，日本原子力研究所が不定期に公刊している研究報告書です。
入手の問合わせは，日本原子力研究所技術情報部情報資料課（〒319-11茨城県那珂郡東海村）あて，お申しこしください。なお，このほかに財団法人原子力弘済会資料センター（〒319-11 茨城県那珂郡東海村日本原子力研究所内）で複写による実費頒布をおこなっております。

JAERI-M reports are issued irregularly.
Inquiries about availability of the reports should be addressed to Information Division Department of Technical Information, Japan Atomic Energy Research Institute, Tokai-mura, Naka-gun, Ibaraki-ken 319-11, Japan.

編集兼発行　日本原子力研究所
印　　刷　いばらき印刷㈱

JAERI-M 93-224

Simulation of Tearing Mode Stabilization by using ECH

Gen-ichi KURITA, Takashi TUDA, Masafumi AZUMI and Tatsuoki TAKEDA

Department of Fusion Plasma Research
Naka Fusion Research Establishment
Japan Atomic Energy Research Institute
Naka-machi, Naka-gun, Ibaraki-ken

(Received October 14, 1993)

Nonlinear simulations based on the reduced set of resistive MHD equations with the transport equation of electron temperature are carried out to investigate the effect of electron temperature perturbation induced by local heating of ECH on a tearing mode activity. Effect of poloidal plasma rotation is also considered in the simulations. It is shown that the local heating can suppress low-m tearing mode instability when O-point of the rotating magnetic island is effectively heated. Large parallel heat conduction causes the radially extending heat deposition profile for small width of magnetic island and magnitude of parallel heat conduction determines the heat power necessary for complete stabilization of the tearing mode.

Keywords: Nonlinear Simulation, Tearing Mode, Reduced MHD, ECH, Heating Power, Magnetic Island Rotation, Parallel Heat Conduction

JAERI-M 93-224

ＥＣＨによるテアリング・モード安定化のシミュレーション

日本原子力研究所那珂研究所炉心プラズマ研究部
栗田　源一・津田　　孝・安積　正史・竹田　辰興

（1993年10月14日受理）

ＥＣＨの局所加熱によって引き起こされる電子温度の摂動のテアリング・モードに対する効果を調べるために，電子温度輸送方程式を伴った簡約抵抗性ＭＨＤ方程式に基づくシミュレーションを行った。シミュレーションにおいて，ポロイダル・プラズマ回転の効果も考慮されている。

もし回転する磁気島の０点が効率的に加熱に加熱されれば，局所加熱によって低mのテアリング・モードを完全に安定化できることを示した。小さな幅の磁気島に対して，磁力線方向の大きな熱伝導は径方向に伸びたデポジション分布を作り出し，またその熱伝導の大きさがテアリング・モードを完全に安定化するために必要な加熱入力を決定する。

那珂研究所：〒311－01　茨城県那珂郡那珂町大字向山801－１

Contents

1. Introduction 1
2. Basic Equations and Numerical Procedure 2
3. Stabilization Condition 5
3.1 Evolution of Magnetic Island Width 5
3.2 Simulations 9
4. Local Heating Effect on Saturated Magnetic Island 12
5. Local Heating Effect on Rotating Magnetic Island 15
6. Summary and Discussions 17
Acknowledgments 18
References 19

目　　次

1. はじめに 1
2. 基礎方程式と数値手続き 2
3. 安定化条件 5
3.1 磁気島幅の発展 5
3.2 シミュレーション 9
4. 飽和磁気島に対する局所加熱の効果 12
5. 回転磁気島に対する局所加熱の効果 15
6. まとめと討論 17
謝　　辞 18
参 考 文 献 19

1. INTRODUCTION

For achievement of thermonuclear fusion reactor using tokamak, there are many problems to be solved, and the major disruption, which limits the maximum plasma current and the plasma density[1-4], is one of the most important problem among them. An m=2 (m;poloidal mode number) tearing mode is considered to be responsible to this major disruption process, and the suppression of the m=2 tearing mode in a tokamak is an urgent target to be accomplished, because it could provide not only disruption-free operation at relatively low q_a values, but also an improvement in confinement by allowing increased total plasma current.

There have been many proposals to suppress the m=2 tearing mode, for example, by externally applied resonant helical field using negative feedback[5-8]. The feedback control is very powerful means if it is possible to determine precisely the phase of the magnetic island and if the time required to produce a feedback field is short enough to avoid phase instability. The local heating by ECH just near the singular surface proposed by Yoshioka et al.[9] has been performed in JFT-2M tokamak, recently[10,11]. It is shown that the m=2 tearing mode can be completely stabilized by ECH if the q=2 resonant surface is effectively heated. The local heating of ECH is also applied to the m=1 mode and the sawteeth oscillation is successfully stabilized[12]. The purpose of this research is to investigate the effect of local heating on the m=2 tearing mode activity, to clarify the mechanism of stabilizing effect, for example, which has more important role in the stabilization, the heating of O-point, where the helical poloidal flux function has its maximum value, of magnetic island[9,13,14] or the background modification of m/n=0/0 current density profile[15-17]. To this end, the calculations using the equation of magnetic island evolution and the simulations based on the reduced set of resistive MHD equations are carried out. The latter includes the transport equation of electron temperature and

the local heating affects the MHD activity through the perturbation of plasma resistivity . The tearing mode activity with the local heating are also studied extensively by the simulations.

In Section 2, the basic equations and numerical procedure are briefly described. In Section 3, condition of the stabilization is investigated analytically on the basis of the equation of magnetic island evolution, and also numerically by the simulations. The simulations to study the effect of local heating on saturated magnetic island are carried out in Section 4. In Section 5, local heating effect on rotating magnetic island, as in usual condition of experiments, are also studied by the simulations. The discussion and conclusions are given in Section 6.

2. BASIC EQUATIONS AND NUMERICAL PROCEDURE

As basic equations, we employ the reduced set of resistive MHD equations of a low β, cylindrical tokamak[18,19] with the transport equation of electron temperature. The equations with the assumption of helical symmetry are shown as follows,

$$\frac{\partial U}{\partial t} = -(\vec{v}_\perp \cdot \vec{\nabla}_\perp)U + (\vec{B}^* \cdot \vec{\nabla}_\perp)U + \nu \Delta_\perp U \quad , \tag{1}$$

$$\frac{\partial \psi^*}{\partial t} = -(\vec{v}_\perp \cdot \vec{\nabla}_\perp)\psi^* + \eta J - E \quad , \tag{2}$$

$$\frac{\partial T_e}{\partial t} = -(\vec{v}_\perp \cdot \vec{\nabla}_\perp)T_e + (\vec{B}^* \cdot \vec{\nabla}_\perp)\left\{\kappa_\parallel (\vec{B}^* \cdot \vec{\nabla}_\perp)T_e\right\} + \vec{\nabla}_\perp \cdot (\kappa_\perp \vec{\nabla}_\perp T_e) + g\eta J^2 + h \quad , \tag{3}$$

$$J = \Delta_\perp \psi^* + \frac{2n}{m} \quad , \tag{4}$$

$$U = \Delta_\perp \phi \quad , \tag{5}$$

the local heating affects the MHD activity through the perturbation of plasma resistivity . The tearing mode activity with the local heating are also studied extensively by the simulations.

In Section 2, the basic equations and numerical procedure are briefly described. In Section 3, condition of the stabilization is investigated analytically on the basis of the equation of magnetic island evolution, and also numerically by the simulations. The simulations to study the effect of local heating on saturated magnetic island are carried out in Section 4. In Section 5, local heating effect on rotating magnetic island, as in usual condition of experiments, are also studied by the simulations. The discussion and conclusions are given in Section 6.

2. BASIC EQUATIONS AND NUMERICAL PROCEDURE

As basic equations, we employ the reduced set of resistive MHD equations of a low β, cylindrical tokamak[18,19] with the transport equation of electron temperature. The equations with the assumption of helical symmetry are shown as follows,

$$\frac{\partial U}{\partial t} = -(\vec{v}_\perp \cdot \vec{\nabla}_\perp)U + (\vec{B}^* \cdot \vec{\nabla}_\perp)U + \nu \Delta_\perp U \quad , \tag{1}$$

$$\frac{\partial \psi^*}{\partial t} = -(\vec{v}_\perp \cdot \vec{\nabla}_\perp)\psi^* + \eta J - E \quad , \tag{2}$$

$$\frac{\partial T_e}{\partial t} = -(\vec{v}_\perp \cdot \vec{\nabla}_\perp)T_e + (\vec{B}^* \cdot \vec{\nabla}_\perp)\left\{\kappa_\parallel (\vec{B}^* \cdot \vec{\nabla}_\perp)T_e\right\} + \vec{\nabla}_\perp \cdot (\kappa_\perp \vec{\nabla}_\perp T_e) + g\eta J^2 + h \quad , \tag{3}$$

$$J = \Delta_\perp \psi^* + \frac{2n}{m} \quad , \tag{4}$$

$$U = \Delta_\perp \phi \quad , \tag{5}$$

$$\vec{v}_\perp = \vec{e}_z \times \nabla_\perp \phi \quad , \tag{6}$$

$$\vec{B}^* = \vec{e}_z \times \nabla_\perp \psi^* \quad , \tag{7}$$

where U, $\vec{v}_\perp$, $\vec{B}^*$, J, ν, ψ^*, η, E, T_e, $\kappa_\parallel$, $\kappa_\perp$, g, h are vortex, plasma velocity, helical magnetic field, current density, viscosity, helical poloidal flux function, plasma resistivity, electric field, electron temperature, heat conduction coefficients parallel and perpendicular to magnetic field, coefficient of joule heating and heating source term, respectively, and m, n and $\vec{e}_z$ are poloidal, toroidal mode numbers and unit vector in z direction, respectively. The parallel and perpendicular thermal conduction coefficients are functions of electron temperature as $\kappa_\parallel = \kappa_{\parallel 0} T_e^{f_\parallel}$ and $\kappa_\perp = \kappa_{\perp 0} T_e^{f_\perp}$. The electron temperature perturbation, Eq.(3), affects MHD phenomena, Eqs.(1) and (2), through plasma resistivity perturbation, which is obtained by using Spitzer's conductivity relation; $\eta = \kappa_S T_e^{-2/3}$. In these equations, uniform plasma density is assumed and the time is normalized to the poloidal Alfvén transit time $\tau_{pa} = \sqrt{\rho} R / B_t$ (with ρ the plasma density, R the major radius and B_t the toroidal magnetic field), which is, in other word, the major radius divided by toroidal Alfvén velocity. All lengths are normalized to the plasma minor radius a, and the electron temperature is normalized in such a way that the Spizter's coefficient $\kappa_S = 1$ as $\eta = T_e^{-3/2}$. The above set of non-linear equations is solved with the predictor-corrector time integration scheme. The viscosity term in Eq.(1) and the diffusion term in Eq.(2) and also the parallel and perpendicular conduction terms in Eq.(3), are approximated by the full implicit representation. All variables are Fourier expanded about poloidal and toroidal directions. To include the rotation effect of plasma, all variables are treated as complex numbers in the simulations in Section 5. Therefore, the effect of feedback control of local heating can be included consistently as in the experiments[11].

The boundary conditions necessary for numerical integration of Eqs.(1)-(3) are as follows; $U'_{0/0}$, $\Phi'_{0/0}$, $T'_{0/0}$, $\Psi'_{0/0}=0$ at r=0, $U_{0/0}$, $\Phi_{0/0}$, $T_{0/0}$, $\Psi'_{0/0}$=const. at r=a, and $U_{m/n}$, $\Phi_{m/n}$, $T_{m/n}$, $\Psi_{m/n}=0$ at r=0 and r=a.

The initial profiles of the safety factor is chosen as

$$q(r)=q_0\left[1+(r/r_0)^{2\lambda}\right]^{1/\lambda} \quad . \tag{8}$$

The initial poloidal flux function $\Psi_{0/0}$ is obtained by integrating r^2/q with respect to r, and the equilibrium current profile can be calculated with Eq.(4) using $\Psi_{0/0}$. Then, the resistivity profile $\eta_{0/0}(r)$ is obtained from the condition $\eta_{0/0}(r)J_{0/0}(r)$=const., from which the initial electron temperature profile is determined. The initial profile of the stream function is chosen as

$$\Phi_{0/0}=\Phi_{a0}\left[1-(r/a)^{\chi}\right] \quad , \tag{9}$$

where $\Phi_{a0}=-2\pi/(\chi\tau_s)$ and τ_S is initial period of plasma rotation at the plasma surface.

We adopt the following local heating profile, $h(r,\theta)$, in two dimensional real space for simplicity, unless otherwise noted, where θ is the helical coordinate expressed by poloidal angle, Θ, and toroidal angle, ϕ, as $\theta=\Theta-(n/m)\phi$. The heat profile divided by the value of electron temperature at the magnetic axis is

$$h(r,\theta)=P_{rf}(1-f(r,\theta)^{h_1})^{h_2} \quad ; \quad f(r,\theta)\le 1 \quad , \tag{10}$$

$$h(r,\theta)=0 \quad ; \quad f(r,\theta)>1 \quad , \tag{11}$$

with

$$f(r,\theta)=\left(\frac{r-r_\delta(t)}{\delta_r}\right)^2+\left(\frac{\theta-\theta_\delta}{\delta_\theta}\right)^2 \quad , \tag{12}$$

where, P_{rf}, h_1, h_2, δ_r, δ_θ, $r_{\delta(t)}$ and $\theta\delta$ denote amplitude, peaking factor, broadening factor, width of radial,

poloidal directions, radial and poloidal positions of the heat deposition profile, respectively. The radial position, of the deposition center, $r_\delta(t)$, can be changed in time according to the position of resonant surface. The heating power is turned on during the time interval; $t_{hs}<t<t_{he}$.

The equilibrium and numerical parameters in the simulations carrying out in sections 3., 4. and 5 are in the following; as the equilibrium parameters, we use $q_0=1.2$, $\lambda=2$, $r_0=0.606$ in Eq.(8), where q=2 resonant surface is located at $r_s=0.7$ and the safety factor at the plasma surface is $q_a=3.48$. The values of viscosity, plasma resistivity and parallel and perpendicular conduction are $\nu=10^{-5}$, $\eta(r_s)=5\times10^{-5}$, $\kappa_{\parallel}(0)=10^2$ with $f_{\parallel}=2.5$ and $\kappa_{\perp}=10^{-5}$ with $f_{\perp}=0$, and for the peaking and broadening factors of heating profile, we choose $h_1=2.5$ and $h_2=1.5$ in Eq.(10), unless otherwise noted. The coefficient of Joule heating is set to be zero($g=0$ in Eq.(3)), for simplicity, because it is not so important for m=2 tearing mode activity. The simulations are carried out with 200 radial grids with regular intervals and 10 single helicity Fourier modes.

3. STABILIZATION CONDITION

In this section, the stabilization mechanism of the m=2 tearing mode by means of local heating is investigated. In subsection (3.1), the equation of magnetic island evolution using Δ' value[12,19,20] is extended to include effect of large parallel conductivity, and the simulations to obtain the stabilization condition and also to check the applicability of the extended equation of magnetic island are carried out in subsection (3.2).

3.1 Evolution of magnetic island width

In this subsection, we extend the equation of magnetic island evolution with the effect of electron temperature perturbation[9,13] under the effect of large parallel

poloidal directions, radial and poloidal positions of the heat deposition profile, respectively. The radial position, of the deposition center, $r_\delta(t)$, can be changed in time according to the position of resonant surface. The heating power is turned on during the time interval; $t_{hs}<t<t_{he}$.

The equilibrium and numerical parameters in the simulations carrying out in sections 3., 4. and 5 are in the following; as the equilibrium parameters, we use $q_0=1.2$, $\lambda=2$, $r_0=0.606$ in Eq.(8), where q=2 resonant surface is located at $r_s=0.7$ and the safety factor at the plasma surface is $q_a=3.48$. The values of viscosity, plasma resistivity and parallel and perpendicular conduction are $\nu=10^{-5}$, $\eta(r_s)=5\times10^{-5}$, $\kappa_{\parallel}(0)=10^2$ with $f_{\parallel}=2.5$ and $\kappa_{\perp}=10^{-5}$ with $f_{\perp}=0$, and for the peaking and broadening factors of heating profile, we choose $h_1=2.5$ and $h_2=1.5$ in Eq.(10), unless otherwise noted. The coefficient of Joule heating is set to be zero($g=0$ in Eq.(3)), for simplicity, because it is not so important for m=2 tearing mode activity. The simulations are carried out with 200 radial grids with regular intervals and 10 single helicity Fourier modes.

3. STABILIZATION CONDITION

In this section, the stabilization mechanism of the m=2 tearing mode by means of local heating is investigated. In subsection (3.1), the equation of magnetic island evolution using Δ' value[12,19,20] is extended to include effect of large parallel conductivity, and the simulations to obtain the stabilization condition and also to check the applicability of the extended equation of magnetic island are carried out in subsection (3.2).

3.1 Evolution of magnetic island width

In this subsection, we extend the equation of magnetic island evolution with the effect of electron temperature perturbation[9,13] under the effect of large parallel

conductivity. The evolution of magnetic island width, w, is obtained by integrating Eq.(2) along the flux surface inside the magnetic island as;

$$\frac{dw}{dt} = \eta\left[C_1\Delta'(w) + \frac{C_2}{\tilde{\psi}_m}\frac{j_0}{\eta_0}\int_{-w/2}^{w/2}\tilde{\eta}_m dr\right] \quad , \tag{13}$$

where j_0 and η_0 are equilibrium current density and plasma resistivity and $\tilde{\psi}_m$ and $\tilde{\eta}_m$ are perturbed poloidal flux function and plasma resistivity perturbation induced by local heating. In Eq.(13), $\Delta'(w)$ is,

$$\Delta'(w) = \frac{\psi'(r_s + w/2) - \psi'(r_s - w/2)}{\psi(r_s)} \quad , \tag{14}$$

where the prime denotes the derivative with respect to r, and r_s is the position of singular surface. The constants C_1 and C_2 in Eq.(13) are constants of order 1, which are obtained by the averaging procedure in poloidal direction within the magnetic island region. We set C_1=1 in the following for simplicity. In this subsection, we adopt the following heat profile,

$$h(r,\theta) = \hat{P}_{rf}(r)\cos(m\theta) \quad , \tag{15}$$

where $\hat{P}_{rf}(r)$ has finite constant value, P_{rf}(heat power), only in the region, $2|r-r_s|<\delta_r$, where δ_r is the radial width of heat profile. This form of heat profile, which corresponds to O-point heating and X-point cooling, is considered to be the most effective one to stabilize tearing mode[13]. In the following, we consider the three cases classified according to the size of magnetic island, w: Case(a); $w > \delta_r$, Case(b); $\delta_{||} < w < \delta_r$ and Case(c); $w < \delta_{||}$, where $\delta_{||}$ is the region, where the effect of large parallel conduction on the deposition of the local heating is ineffective in the diffusion process of the local heating source term near the singular surface ($2|r-r_s|<\delta_{||}$), and is expressed as,

$$\delta_{||} \approx \left(\frac{\kappa_\perp}{\kappa_{||}}\right)^{1/4}\left(\frac{r_s L_s}{m}\right)^{1/2} \quad , \tag{16}$$

where $L_S (\cong Rq^2/rq')$ is the shear length along the magnetic field line. Equation (16) is obtained by Eq.(3) with the condition of steady state. In the case(a), we can set the perturbation of electron temperature, $\tilde{T}_m$, to be zero at $2|r-r_S|>w$, because the input power in the interior of magnetic island is constant, and does not depend on the width of the magnetic island, w,. In the second case(b), the input power in the interior of magnetic island decreases with that of the width of magnetic island, and we can set $\tilde{T}_m=0$ at $2|r-r_S|>w$ as in the previous case. Finally, we consider the case(c). In the region considered in this case, the perturbation of electron temperature is determined by the width of $\delta_{\parallel}$, and does not depend on w.

After replacing the plasma resistivity perturbation by that of electron temperature using Spitzer's conductivity relation; $\tilde{\eta}_m/\eta_0 = -(3/2)(\tilde{T}_m/T_0)$ in Eq.(13), and integrating it within the island width with each conditions mentioned above, we get the following three equations of magnetic island according to the width of magnetic island,

$$\frac{dw}{dt} = \eta\left[\ \Delta'(w) - C_h \frac{P_{rf}}{\kappa_{\perp} T_e}\delta_r\ \right] \qquad ; \quad \delta_{\parallel} << \delta_r < w \ , \qquad (17)$$

$$\frac{dw}{dt} = \eta\left[\ \Delta'(w) - C_h \frac{P_{rf}}{\kappa_{\perp} T_e} w\ \right] \qquad ; \quad \delta_{\parallel} < w < \delta_r \ , \qquad (18)$$

$$\frac{dw}{dt} = \eta\left[\ \Delta'(w) - C_h \frac{P_{rf}}{\kappa_{\perp} T_e}\frac{\delta_{\parallel}^2}{w}\ \right] \qquad ; \quad w < \delta_{\parallel} << \delta_r \ , \qquad (19)$$

where the coefficient C_h is determined by the equilibrium quantities as;

$$C_h = \frac{3}{4}\frac{rJ_z}{B_\theta}\frac{q}{rq'}\bigg|_{r=r_s} \ . \qquad (20)$$

The coefficient of 3/4, including the constant C_2 in Eq.(13), of the right hand side of Eq.(20) is numerically estimated value in Ref.[13], the analysis of which is

equivalent to the second case, Eq.(18). The value of C_h is about 0.42 for the equilibrium considered in this paper.

If the magnetic island evolves according to Eq.(18), the local heating effect also vanishes with vanishing w($w \to 0$). Therefore, the complete stabilization of tearing mode, i.e., complete elimination of magnetic island, need infinite heating power. The situation contradicts the results of experiments[10]. On the other hand, we can easily expect complete stabilization in the third case(Eq.(19)) because of w^{-1} dependence of heating effect. This inverse proportionality of dw/dt to w is the same as current drive case[13]. Typical heat power for the saturation of magnetic island width for these three cases are shown in Fig.(1). In these calculations, we assume the function of $\Delta'(w)$ as,

$$\Delta'(w) = \Delta'_0 (1 - \frac{w}{w_0}) \quad , \qquad (21)$$

where Δ'_0 is Δ'(w=0) and w_0 is the saturation width of magnetic island without heating. At first, the necessary heat power for the saturation increases with the decrement of w from w_0 until the width decreases to δ_r. Then, the increment of the necessary power becomes larger because $P_{rf} \propto w^{-1}$ in the region $\delta_\parallel < w < \delta_r$, and finally it reaches maximum value at $w=w_0/2$ in the region $0 < w < \delta_\parallel$, if $w_0/2 \le \delta_\parallel$. Equation (19) has no solution in the region $w<w_0/2$. In the case of $w_0/2 > \delta_\parallel$, Eq.(19) has no solution except $w=\delta_\parallel$, which determines the value of $P_{rf,max}$, i.e., the maximum heat power for the island saturation. $P_{rf,max}$ can be written according to the value of $\delta_\parallel$ in the following;

$$P_{rf,\max} = \frac{\kappa_\perp T_e \Delta'_0}{C_h} \frac{w_0}{4\delta_\parallel^2} \quad ; \quad \frac{w_0}{2} \le \delta_\parallel \quad , \qquad (22)$$

$$P_{rf,\max} = \frac{\kappa_\perp T_e \Delta'_0}{C_h} \left(\frac{1}{\delta_\parallel} - \frac{1}{w_0} \right) \quad ; \quad \delta_\parallel < \frac{w_0}{2} \quad . \qquad (23)$$

$P_{rf,max}$ denoted by Eqs.(22) and (23) are shown by the bold line with arrows and numbers 1 and 2 in Fig.(1),

respectively. If the heating power, P_{rf}, becomes greater than $P_{rf,max}$, the maximum heating power for the island saturation, the plasma encounters the catastrophic change of the phase of magnetic island O-point, and new magnetic islands appear in the opposite phase. These phenomena, which we call "phase inversion", will be shown in the simulations in next subsection(3.2) and Section 4 for the case of non-rotating magnetic island. In the real situation, however, the plasma rotates in toroidal and/or poloidal directions, and the magnetic islands always encounter the stabilizing effect of local heating, when the poloidal position of O-point of the magnetic island almost coincides with that of local heating. In this case, there is no phase inversion, as shown in the simulations in Section 5. Therefore, for the tearing mode to be completely stabilized, heating power must be greater than $P_{rf,max}$, and the magnetic island must rotate in toroidal and/or poloidal directions. It is to be noted that as the value of $\delta_{\parallel}$ becomes smaller, the power necessary for complete stabilization becomes larger. The dependency of T_e on the parameter $\delta_{\parallel}$ is $\delta_{\parallel} \propto T_e^{-3/4}$, where we use the classical dependencies of the thermal conductivity on electron temperature.

3.2 Simulations

The simulations of local heating effect on tearing mode activity are carried out to obtain the stabilization condition and to check the applicability of the equation of the width of magnetic island derived in the previous subsection.

There are proposed two main stabilization mechanisms by local heating, one due to the modification of plasma current profile of m/n=0/0 component and the other due to that of m/n=2/1 component. The former is related to the value of $\Delta'(w)$, and the latter O-point of magnetic island heating. To investigate which has dominant effect on the

stability of tearing mode, we consider the following four cases;

Case I: no heating ($P_{rf}=0$).

Case II: poloidally localized heating with profile of Eqs.(10~12) with $\delta_\theta=\pi/10$ ($P_{rf}=5.5\times10^{-4}$)

Case III: almost poloidally symmetric heating with profile of Eqs.(10~12) with $\delta_\theta=\pi/2$ ($P_{rf}=5.5\times10^{-4}$)

Case IV: heating with profile of Eq.(15) ($P_{rf}=10^{-4}$)

In Case IV, we adopt the same radial dependence of the function for $\hat{P}_{rf}(r,\theta)$ as that in Eq.(12). The heat powers , P_{rf}, of the Case II and III are adjusted to have the same stabilizing effect as in the Case IV. The results are shown in Fig.(2), where Fig.(2.a) and Fig(2.b) show the evolution of the width of magnetic island and the evolution of $\Delta'(w)$, respectively, and Fig.(2.c) and Fig.(2.d) show the evolutions of amplitude of electron temperature and current density of m=2 component at the resonant surface, respectively. The dotted, solid, broken and dotted solid curves in each subfigure correspond to the Cases I, II, III and IV, respectively. In almost poloidally symmetric heat case(Case III), the change of $\Delta'(W)$ is much larger than other two heat cases (See dotted solid curve in the figure). This change of $\Delta'(w)$, however, has little contribution to the stabilization of the tearing mode as shown in Fig.(2.a). The evolutions of electron temperature and current density of m=2 component at $r=r_s$, shown in Fig.(2.c) and (2.d), shows that the increment of $T_m(r_s)$ also increases the current density at the resonant surface and stabilizes the tearing mode. The stabilizing mechanisms of tearing mode by the increased current density are described in Ref.[13]. If the tearing mode is completely stabilized by the local heating, the stabilizing effect is turned into the destabilizing one for the tearing mode in opposite phase, which leads to the phase inversion. The

profiles of electron temperature and current density of the m=2 mode at t=130, when the width of magnetic island becomes almost zero, are shown in Fig.(3) for each cases in Fig.(2). The amplitude of the m=2 component for heating profile of Case II and III are about 7.7×10^{-5} and 9.5×10^{-5}, respectively, both of which are almost the same as 10^{-4} for the Case IV. Therefore, the amplitude of m=2 component determines the effect of heating. It is impossible to give the pure m=2 component of electron temperature perturbation, the local heating only near the O-point of the magnetic island can be said to be essential.

To show the phase inversion phenomenon clearly, we carried out another simulation with different turning on time of heating: t_{hs} (t_{hs}=500), using heat profile of Eq.(15) with $P_{rf}=10^{-4}$, while, in the above simulations, the heating power is turned on at t=0 (t_{hs}=0). The evolutions of the magnetic island width and contour of helical poloidal flux are shown in Fig.(4). The evolution of helical poloidal flux function shows the phase inversion of magnetic island between t=1200 and t=3500.

Next, we describe the simulations performed to check the applicability of Eqs.(17~19). As the difference between Eqs.(17) and (18) is not essential, only the difference between Eqs.(18) and (19) is considered in the following. As for the heating profile, we adopt Eq.(15) for simplicity. We show the evolutions of magnetic island in Fig.(5) for two different heat power, $P_{rf}=10^{-4}$ and 3×10^{-5}, and no heating for broken, solid and dotted curves, respectively. While, the solid curve ($P_{rf}=3\times10^{-5}$) shows the saturation of magnetic island with smaller size compared with the case of no heating(dotted curve) the broken curve ($P_{rf}=10^{-4}$) shows "phase inversion". We show the dependency of heat power P_{rf} on the saturation size of the magnetic island by solving Eq.(18) in Fig.(6). In these calculations, we use the function Δ' of w obtained in the simulation results. Two closed circles with the characters s and b in the figure correspond to solid and broken curves

in Fig.(5), respectively. To explain the phase inversion of broken curve in Fig.(5), we need Eq.(19). To check the applicability of Eq.(19), we must show that $P_{rf,max}$ is the function of $\delta_{\parallel}$, by the simulation. To this end, the simulations with larger value of parallel conductivity, $\kappa_{\parallel}(0)=10^4$, are carried out. Time evolutions of the width of magnetic island are shown in Fig.(7), where Fig.(7.a),(7.b) and (7,c) are the cases with the heat powers; $P_{rf}=10^{-4}$, 3×10^{-4} and 10^{-3}, respectively. It is easily seen from the figure, that the large parallel conduction makes the heat power necessary for the phase inversion larger, which is considered due to smaller value of $\delta_{\parallel}$. The value of $\delta_{\parallel}$ becomes about 0.3 times, and smaller than the simulation with $\kappa_{\parallel}(0)=10^2$, of which the estimated value of $\delta_{\parallel}$ is almost 0.05. The perpendicular diffusion induced by this large parallel conduction coefficient with perturbed radial magnetic field is about 2×10^{-6} and even less than the perpendicular one, $\kappa_{\perp}=10^{-5}$. Therefore, it is shown that the $P_{rf,max}$ is the function of $\delta_{\parallel}$, and it can be said that Eqs. (17-19) explain the results of the simulations.

4. LOCAL HEATING EFFECT ON SATURATED MAGNETIC ISLAND

In this section, the effect of local heating on the saturated magnetic island without plasma rotation is investigated by the simulations. The dependencies of the radial and poloidal positions of heating on the stabilization of the tearing mode are investigated extensively.

We adopt the heat profile of Eq.(10~12), in this section, where the parameters are chosen as $P_{rf}=5\times10^{-3}$, $\delta_r=0.05$, $r_\delta=r_s+\delta_{rs}$, $\delta_\theta=\pi/10$, We carried out the simulations changing the parameters of δ_{rs} and θ_δ in the following. We first show the results of $\delta_{rs}=\theta_\delta=0$ in Fig.(8), where the evolutions of (a) magnetic island and (b) magnetic energy of each mode are shown. The heat power is turned on at t=1500, when the magnetic islands are in saturation state. The evolution of magnetic island width shows rapid stabilization, and becomes zero (w=0) at t=2037, which

in Fig.(5), respectively. To explain the phase inversion of broken curve in Fig.(5), we need Eq.(19). To check the applicability of Eq.(19), we must show that $P_{rf,max}$ is the function of $\delta_{\parallel}$, by the simulation. To this end, the simulations with larger value of parallel conductivity, $\kappa_{\parallel}(0)=10^4$, are carried out. Time evolutions of the width of magnetic island are shown in Fig.(7), where Fig.(7.a),(7.b) and (7,c) are the cases with the heat powers; $P_{rf}=10^{-4}$, 3×10^{-4} and 10^{-3}, respectively. It is easily seen from the figure, that the large parallel conduction makes the heat power necessary for the phase inversion larger, which is considered due to smaller value of $\delta_{\parallel}$. The value of $\delta_{\parallel}$ becomes about 0.3 times, and smaller than the simulation with $\kappa_{\parallel}(0)=10^2$, of which the estimated value of $\delta_{\parallel}$ is almost 0.05. The perpendicular diffusion induced by this large parallel conduction coefficient with perturbed radial magnetic field is about 2×10^{-6} and even less than the perpendicular one, $\kappa_{\perp}=10^{-5}$. Therefore, it is shown that the $P_{rf,max}$ is the function of $\delta_{\parallel}$, and it can be said that Eqs. (17-19) explain the results of the simulations.

4. LOCAL HEATING EFFECT ON SATURATED MAGNETIC ISLAND

In this section, the effect of local heating on the saturated magnetic island without plasma rotation is investigated by the simulations. The dependencies of the radial and poloidal positions of heating on the stabilization of the tearing mode are investigated extensively.

We adopt the heat profile of Eq.(10~12), in this section, where the parameters are chosen as $P_{rf}=5\times10^{-3}$, $\delta_r=0.05$, $r_\delta=r_s+\delta_{rs}$, $\delta_\theta=\pi/10$, We carried out the simulations changing the parameters of δ_{rs} and θ_δ in the following. We first show the results of $\delta_{rs}=\theta_\delta=0$ in Fig.(8), where the evolutions of (a) magnetic island and (b) magnetic energy of each mode are shown. The heat power is turned on at t=1500, when the magnetic islands are in saturation state. The evolution of magnetic island width shows rapid stabilization, and becomes zero (w=0) at t=2037, which

leads to phase inversion. As mentioned in the last section and will be shown in the next section, the rotation of the plasma in toroidal and/or poloidal direction inhibits this phase inversion, and we assume that once the width of magnetic island reaches zero, the tearing mode is completely stabilized, in this section. Although, the magnetic energy of each mode shows different reaction after heat power is turned on because of many Fourier components of the local heating, the effect of m=2 component stabilization is dominant in the final stage. Time evolutions of the electron temperature contours and current density contour with their sectional figures at $\theta=0,\pi$, are shown in Fig.(9). In each subfigure of electron temperature contour in Fig.(9), the heat region is denoted by the bold lines on the constant θ line, and the figure shows how the electron temperature in the interior of magnetic island is raised by local heating and decrease the width of magnetic island. The evolutions of contour and the sectional planes of current density, Fig.(9), shows the local current perturbation corresponding to that of electron temperature as predicted by $\tilde{j}_m / j_0 = (2/3)(\tilde{T}_m / T_0)$. These positive current perturbations flowing in the O-point of the magnetic island reduces the width of magnetic island, until it reaches zero, if the heat power is greater than $P_{rf,max}$, the maximum power for the saturation. Even after new magnetic islands appear in the opposite phase, the small magnetic islands remain in the original poloidal position (See Fig.(9)). This magnetic island is caused by the local heating.

Next, we change the value of δ_{rs}, the radial position of heating as in the experiments. Almost the same results are obtained for $\delta_{rs}=\pm 0.04$ as that in the case of $\delta_{rs}=0$. The necessary time for the plasma to be stabilized is smaller for the case of $\delta_{rs}=0.04$ ($t-t_{hs}=537$) than that for $\delta_{rs}=-0.04$ ($t-t_{hs}=613$), because the radial position of heat center for the former case is nearer to the O-point of magnetic island than that for the latter case. In Fig.(10), we show the time evolutions of the width of magnetic island for $\delta_{rs}=-0.08$, Fig.(10.a), and $\delta_{rs}=0.08$, Fig.(10.b). The

dotted region in each subfigure denotes the radial extent of heat profile. After heat power is turned on, the width of magnetic island reduces, but after the center of heating goes out to the exterior of the magnetic island, the stabilizing effect is lost and the finite size of magnetic island saturation appears, for both cases. We carried out the simulations for other 6 values of δ_{rs}; $\delta_{rs}=\pm 0.12$, ± 0.16, ± 0.2. The results of the squared ratio of saturated width of magnetic island , w, to that at t=1500, w_0, versus radial position of heating center are plotted in Fig.(11). The dotted rectangle for each point denotes the radial extent of heat profile, and w_0 in the figure denotes the width of saturated magnetic island without heating. The qualitative good agreement with the experimental results[10] is obtained. The larger stabilizing region compared to that of experiments may be attributed to the large width of magnetic island saturation in the simulations.

Next, we investigate the dependencies of stabilizing effect on poloidal position of the heating, $\theta\delta$. In these simulations, the heat power is turned on at t=1500 as in the previous simulations. The time evolutions of magnetic island with different poloidal position of heating are shown in Fig.(12), where Fig.(12.a), (12.b) and (12.c) show the cases of $\theta\delta=\pi/8$, $\pi/4$ and $\pi/2$, respectively. While, heating with $\theta\delta=\pi/8$ shows fast stabilization, the stabilizing effect of heating with $\theta\delta=\pi/4$ is much smaller than the above case. The contour of electron temperature, current density and the helical poloidal flux at t=3000 of $\theta\delta=\pi/4$ case(Fig.(12.b)) are shown in Fig.(13). In the case of $\theta\delta=\pi/2$, which corresponds to X-point heating, there is little stabilization effect, as shown by Fig.(12.c). Therefore, it is shown that the heating of O-point has a dominant effect in stabilizing process of tearing mode by the local heating.

If the magnetic island is locked at some poloidal position by the error field, and if, furthermore, the heating position is just O-point of the non-rotating

magnetic island, the heating only induce phase inversion. Therefore, to stabilize the tearing mode in non-rotating, locked, plasma by local heating, we must use the feedback control of the poloidal position of heating, which seems very difficult actually.

In the simulations carried out in this section, we use the large input power for the local heating because of CPU limitation of the computer. One run for the case of rotating plasma takes about a few 10 hours of CPU time by using FACOM VP-2600 vector machine. The input power for $P_{rf}=5\times10^{-3}$ $\left((2/\pi)\int_0^{\pi/2} d\theta \int_0^{a} h(r,\theta)\, rdr \cong 2\times10^{-5}\right)$ is about 4 times larger than that of Joule input power $\left(\int_0^{a} \eta_0 J_0^2\, rdr \cong 5\times10^{-6}\right)$. But as shown in the simulation of the previous section, one order lower power, $P_{rf}=5.5\times10^{-4}$, is sufficient for the m=2 tearing mode to be completely stabilized. The input power for ECH in the suppression of disruption experiments is also about a few 10 percent of the Joule input power[11].

5. LOCAL HEATING EFFECT ON ROTATING MAGNETIC ISLAND

In this section, we consider the effect of local heating on rotating magnetic island. The main purpose of the simulations in this section is to show the complete stabilization of the tearing mode instead of phase inversion, which is observed at the final stage of the stabilization in the case of non-rotating magnetic island, and also to show the effect of feedback control to reduce the total heat power.

The initial poloidal flow velocity is determined by Eq.(9) with $\chi=2$, which corresponds to rigid body rotation, and as an initial rotation period, we choose $\tau_s=250$. The amplitude of heat power is chosen as $P_{rf}=3\times10^{-3}$. Other parameters are the same as the simulations in Section 4. The time evolutions of (a) rotating magnetic island width and (b) the poloidal position of magnetic island O-point are shown in Fig.(14). Heat power is turned on at t=1500,

magnetic island, the heating only induce phase inversion. Therefore, to stabilize the tearing mode in non-rotating, locked, plasma by local heating, we must use the feedback control of the poloidal position of heating, which seems very difficult actually.

In the simulations carried out in this section, we use the large input power for the local heating because of CPU limitation of the computer. One run for the case of rotating plasma takes about a few 10 hours of CPU time by using FACOM VP-2600 vector machine. The input power for $P_{rf}=5\times10^{-3}$ $\left((2/\pi)\int_0^{\pi/2} d\theta \int_0^{a} h(r,\theta)\, r dr \cong 2\times10^{-5}\right)$ is about 4 times larger than that of Joule input power $\left(\int_0^{a} \eta_0 J_0^2\, r dr \cong 5\times10^{-6}\right)$. But as shown in the simulation of the previous section, one order lower power, $P_{rf}=5.5\times10^{-4}$, is sufficient for the m=2 tearing mode to be completely stabilized. The input power for ECH in the suppression of disruption experiments is also about a few 10 percent of the Joule input power[11].

5. LOCAL HEATING EFFECT ON ROTATING MAGNETIC ISLAND

In this section, we consider the effect of local heating on rotating magnetic island. The main purpose of the simulations in this section is to show the complete stabilization of the tearing mode instead of phase inversion, which is observed at the final stage of the stabilization in the case of non-rotating magnetic island, and also to show the effect of feedback control to reduce the total heat power.

The initial poloidal flow velocity is determined by Eq.(9) with $\chi=2$, which corresponds to rigid body rotation, and as an initial rotation period, we choose $\tau_s=250$. The amplitude of heat power is chosen as $P_{rf}=3\times10^{-3}$. Other parameters are the same as the simulations in Section 4. The time evolutions of (a) rotating magnetic island width and (b) the poloidal position of magnetic island O-point are shown in Fig.(14). Heat power is turned on at t=1500,

when the rotating magnetic island is in saturation state. The rotating magnetic island completely vanishes at t=3000. In Fig.(15), the time evolution of rotating electron temperature contour is shown. Although, there is seen still small magnetic island in the figure in the region t>3000, it is not induced by the tearing mode but local heating itself, as shown in the simulation of the last section (See subfigure of t=2550 in Fig.(9)). The O-point of the small magnetic island remains about θ=0, where local heating is applied as shown in Fig.(15). If heat power is turned off at t=3000, the magnetic island of small width continues to rotate with the plasma. Furthermore, for the larger heat power, $P_{rf}=10^{-2}$, the width of this steady small magnetic island becomes larger than the case of $P_{rf}=3\times10^{-3}$. After heat power is turned on, t>1500, the maximum change of plasma rotation at the resonant surface is less than 0.05%, and the rigid body rotation of the plasma scarcely changes during the simulation. In contrast with the case of external helical field[22,23], local heating makes little torque, because the heated electrons are instantaneously distributed to each magnetic field lines due to large parallel conduction. The reason why the magnetic island induced by local heating can slip the plasma rotation is also attributed to finite parallel conduction of electron temperature.

As shown in the previous section, to heat O-point of the magnetic island is essential in the stabilizing procedure, there are much extra power for the continuous heating to the rotating magnetic island. Therefore, we try to reduce the power maintaining the same stabilizing effect by using the feedback control. The feedback control has been performed in the experiments already[11], the main purpose of which is different from that of this paper, and is to show that the O-point heating is essential in stabilizing procedure. The feedback conditions used in the simulation is expressed by the following two equations,

$$\left|\psi_{2/1}\right| / \left|\psi_{0/0}\right|_{t=0} > \varepsilon_1 \quad , \qquad (24)$$

$$\left|real(\psi_{2/1})\right| / \left|\psi_{2/1}\right| > \varepsilon_2 \quad . \qquad (25)$$

Equations (24) and (25) are the conditions for the amplitude and the phase of the perturbation of poloidal flux function, respectively. If these two conditions are satisfied, the heat power is supplied at some poloidal position θ_h. The detector coil position is fixed at $\theta=0$, and we can change the phase of heating by the finite value of θ_h.

The results are shown in Fig.(16), where we set $\varepsilon_1=10^{-4}$ and $\varepsilon_2=0.707$ and other parameters are the same as in Fig.(14). Although, heat power is supplied only on the time duration shown by the bold dotted line in the figure, and the total power is about 0.25 times smaller than the continuous heat case, almost the same stabilizing effect is present as that in no feedback. After t=2800, no heat power is supplied because the perturbation of poloidal flux is too small to satisfy Eq.(24).

The feedback control is also performed to heat the X-point ($\theta_h=\pi/2$), as in the experiments. There is no stabilizing effect as easily expected, which is shown by the broken curve in Fig.(16).

6. SUMMARY AND DISCUSSIONS

We carried out the non-linear calculations based on the reduced set of the resistive MHD equations with the transport equation of electron temperature and poloidal plasma rotation to investigate the effect of local heating on the m=2 tearing mode activity. The results obtained are described in the following.

(1) An m=2 tearing mode can be completely stabilized by local heating, if O-point of the magnetic island is effectively heated. The positive current perturbation induced at O-point of magnetic island by the temperature

$$\left|real(\psi_{2/1})\right| / \left|\psi_{2/1}\right| > \varepsilon_2 \quad . \qquad (25)$$

Equations (24) and (25) are the conditions for the amplitude and the phase of the perturbation of poloidal flux function, respectively. If these two conditions are satisfied, the heat power is supplied at some poloidal position θ_h. The detector coil position is fixed at $\theta=0$, and we can change the phase of heating by the finite value of θ_h.

The results are shown in Fig.(16), where we set $\varepsilon_1=10^{-4}$ and $\varepsilon_2=0.707$ and other parameters are the same as in Fig.(14). Although, heat power is supplied only on the time duration shown by the bold dotted line in the figure, and the total power is about 0.25 times smaller than the continuous heat case, almost the same stabilizing effect is present as that in no feedback. After t=2800, no heat power is supplied because the perturbation of poloidal flux is too small to satisfy Eq.(24).

The feedback control is also performed to heat the X-point ($\theta_h=\pi/2$), as in the experiments. There is no stabilizing effect as easily expected, which is shown by the broken curve in Fig.(16).

6. SUMMARY AND DISCUSSIONS

We carried out the non-linear calculations based on the reduced set of the resistive MHD equations with the transport equation of electron temperature and poloidal plasma rotation to investigate the effect of local heating on the m=2 tearing mode activity. The results obtained are described in the following.

(1) An m=2 tearing mode can be completely stabilized by local heating, if O-point of the magnetic island is effectively heated. The positive current perturbation induced at O-point of magnetic island by the temperature

perturbation through that of plasma resistivity reduces the width of magnetic island.

(2) For the small magnetic island, the radially extending heat deposition profile by the local heating is not determined by the magnetic island width, but is determined by the magnitude of the parallel heat conduction, and it avoids the minimum heat power necessary for complete stabilization goes up infinite as the width of magnetic island, $w \rightarrow 0$.

(3) If the magnetic island is locked at some poloidal position by the error field, and if, furthermore, the heat position is just O-point of the static magnetic island, the heating only induce phase inversion, and the new magnetic island appears in the opposite phase. The rotation of poloidal direction inhibit this phase inversion, and keep the plasma in the state without magnetic island due to the tearing mode.

To stabilize the tearing mode in no rotating locked plasma by local heating, we must use the feedback control of the poloidal position of heating, which seems very difficult actually. As mentioned in Ref.[11], the technique to trace the exact radial position of q=2 surface must be developed for long time application of this method. To reduce the heat power, feedback control is very powerful means and it can be reduced to about 0.25 times lower with the same effect than that without feedback control.

ACKNOWLEDGMENTS

The authors would like to express their sincere thanks to Drs. T. Takizuka, K. Hoshino and M. Mori for their fruitful discussions, and also to Dr. M. Tanaka for his continuing encouragement.

perturbation through that of plasma resistivity reduces the width of magnetic island.

(2) For the small magnetic island, the radially extending heat deposition profile by the local heating is not determined by the magnetic island width, but is determined by the magnitude of the parallel heat conduction, and it avoids the minimum heat power necessary for complete stabilization goes up infinite as the width of magnetic island, $w \rightarrow 0$.

(3) If the magnetic island is locked at some poloidal position by the error field, and if, furthermore, the heat position is just O-point of the static magnetic island, the heating only induce phase inversion, and the new magnetic island appears in the opposite phase. The rotation of poloidal direction inhibit this phase inversion, and keep the plasma in the state without magnetic island due to the tearing mode.

To stabilize the tearing mode in no rotating locked plasma by local heating, we must use the feedback control of the poloidal position of heating, which seems very difficult actually. As mentioned in Ref.[11], the technique to trace the exact radial position of q=2 surface must be developed for long time application of this method. To reduce the heat power, feedback control is very powerful means and it can be reduced to about 0.25 times lower with the same effect than that without feedback control.

ACKNOWLEDGMENTS

The authors would like to express their sincere thanks to Drs. T. Takizuka, K. Hoshino and M. Mori for their fruitful discussions, and also to Dr. M. Tanaka for his continuing encouragement.

REFERENCES

[1] SAUTHOFF,N.R., VON GOELER,S., STODIEK,W., Nucl. Fusion **18** (1978) 1445.

[2] TOI,K., ITOH,S., KADOTA,K., et al., Nucl. Fusion **19** (1979) 1643

[3] NAGAMI,M., YOSHIDA,H., SHINYA,K., et al. Nucl. Fusion **22** (1982) 409.

[4] TSUJI,S., NAGAYAMA,Y., MIYAMOTO,K., KAWAHATA,K., NODA, N., TANAHASHI,S., Nucl. Fusion **25** (1985) 305.

[5] HOLMES,J.A., CARRERAS,B.A., HICKS,H.R., LYNCH,S.J., WADDELL,B.V., Nucl. Fusion **19** (1979) 1333.

[6] LAZZARO,E., NAVE,M.F.F, Phys. Fluids **31** (1988) 1623.

[7] BOSIA,G., LAZZARO,E., Nucl. Fusion **31** (1991) 1003.

[8] MORRIS,A.W., HENDER,T.C., HUGILL,J., et al., Phys. Rev. Lett. **64** (1990) 1254

[9] YOSHIOKA,Y., KINOSHITA,S., KOBAYASHI,T., Nucl. Fusion **24** (1984) 565.

[10] HOSHINO,K., MORI,M., YAMAMOTO,T., et al., Phys. Rev. Lett. **69** (1992) 2208.

[11] HOSHINO,K., MORI,M., YAMAMOTO,T., et al., 10th Topical Conf. on RF Power in Plasmas, Boston, April 1993, to be published in AIP conference series.

[12] TANAKA,S., HANADA,K., TANAKA,H., et al., Phys. Fluids **B3** (1991) 2200.

[13] RUTHERFORD,P.H., in Basic Physical Processes of Toroidal Fusion Plasmas(Proc. Course and Workshop Varenna, 1985), Vol.2, CEC, Luxembourg (1986) 531.

[14] KIM,J.S., Chu,M.S., GREEN,J.M., Plasma Phys. Controlled Fusion **30** (1987) 183.

[15] CHAN,V., GUEST,G., Nucl. Fusion **22** (1982) 272.

[16] DE LUCA,F., JACCHIA,A., LAZZARO,E., Phys. Fluids **29** (1986) 501.

[17] WESTERHOF,E., GOEDHEER,W.J., Plasma Phys. Controlled Fusion **30** (1988) 1691.

[18] STRAUSS,H.R., Phys. Fluids **19** (1976) 134.

[19] ROSENBLUTH,M.N., MONTICELLO,D.A., STRAUSS,H.R., WHITE,R.B., Phys. Fluids **19** (1976) 1987.

[20] RUTHERFORD,P.H., Phys. Fluids **16** (1973) 1903.

[21] WHITE,R.B., MONTICELL,D.A., ROSENBLUTH,M.N., WADDELL,B.V., Phys. Fluids **20** (1977) 800.

[22] FITZPATRICK,R., HENDER,T.C., Phys. Fluids **B3** (1991) 644.

[23] KURITA,G., TUDA,T., AZUMI,M., TAKEDA,T., Nucl. Fusion **32** (1992) 1899.

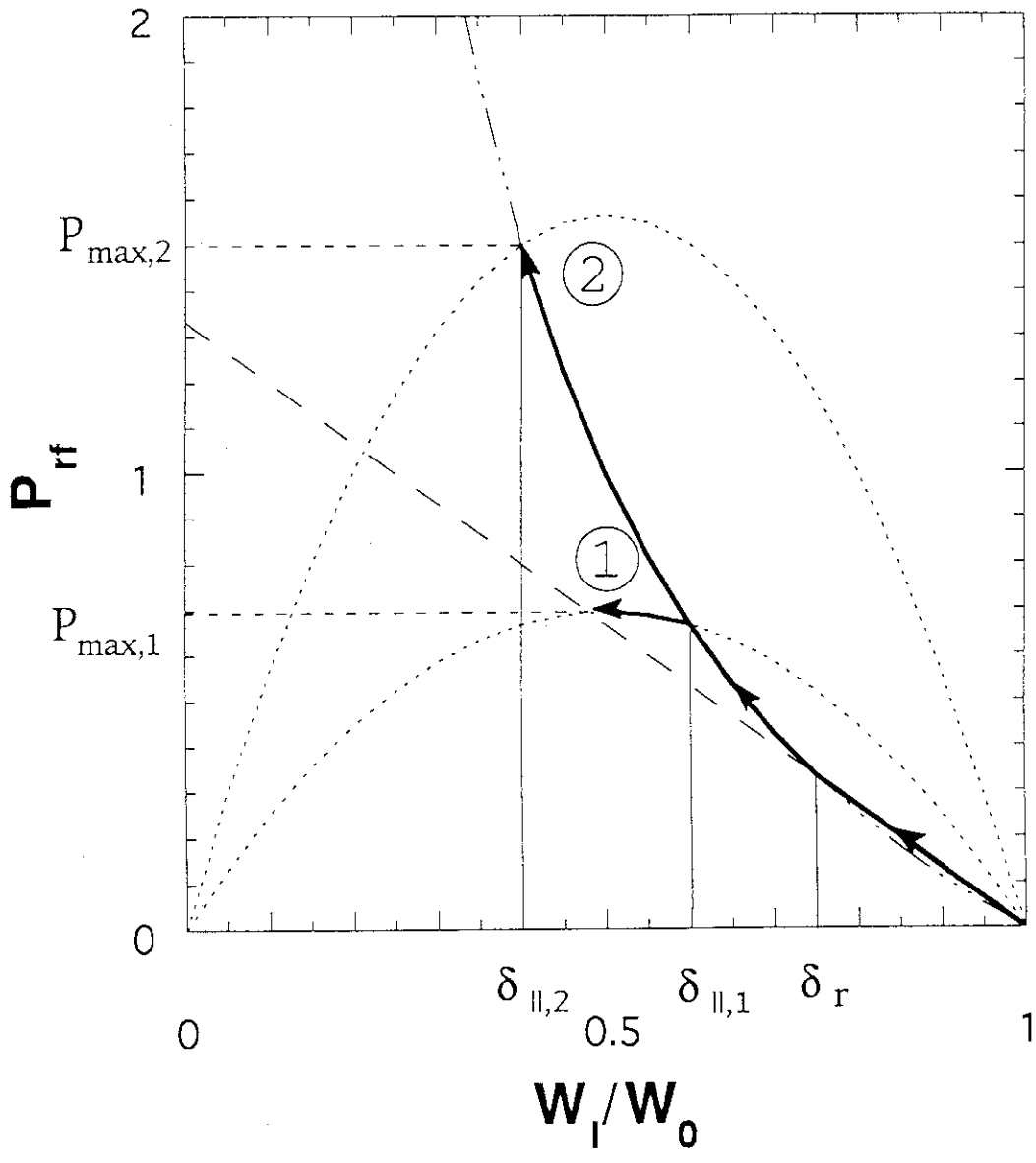

Fig. 1 Necessary normalized heat power for saturation of magnetic island versus width of magnetic island, obtained by Eqs. (17-19). δ_r and $\delta_{\perp\!\!\!\perp}$ denote radial width of heat region and the width of $\kappa_{\perp\!\!\!\perp}$ ineffective region, respectively. w, δ_r and $\delta_{\perp\!\!\!\perp}$ are normalized to the saturation width of magnetic island without heating, w_0. $P_{max,1}$ and $P_{max,2}$ are maximum powers for the existence of solution expressed by Eqs.(22) and (23).

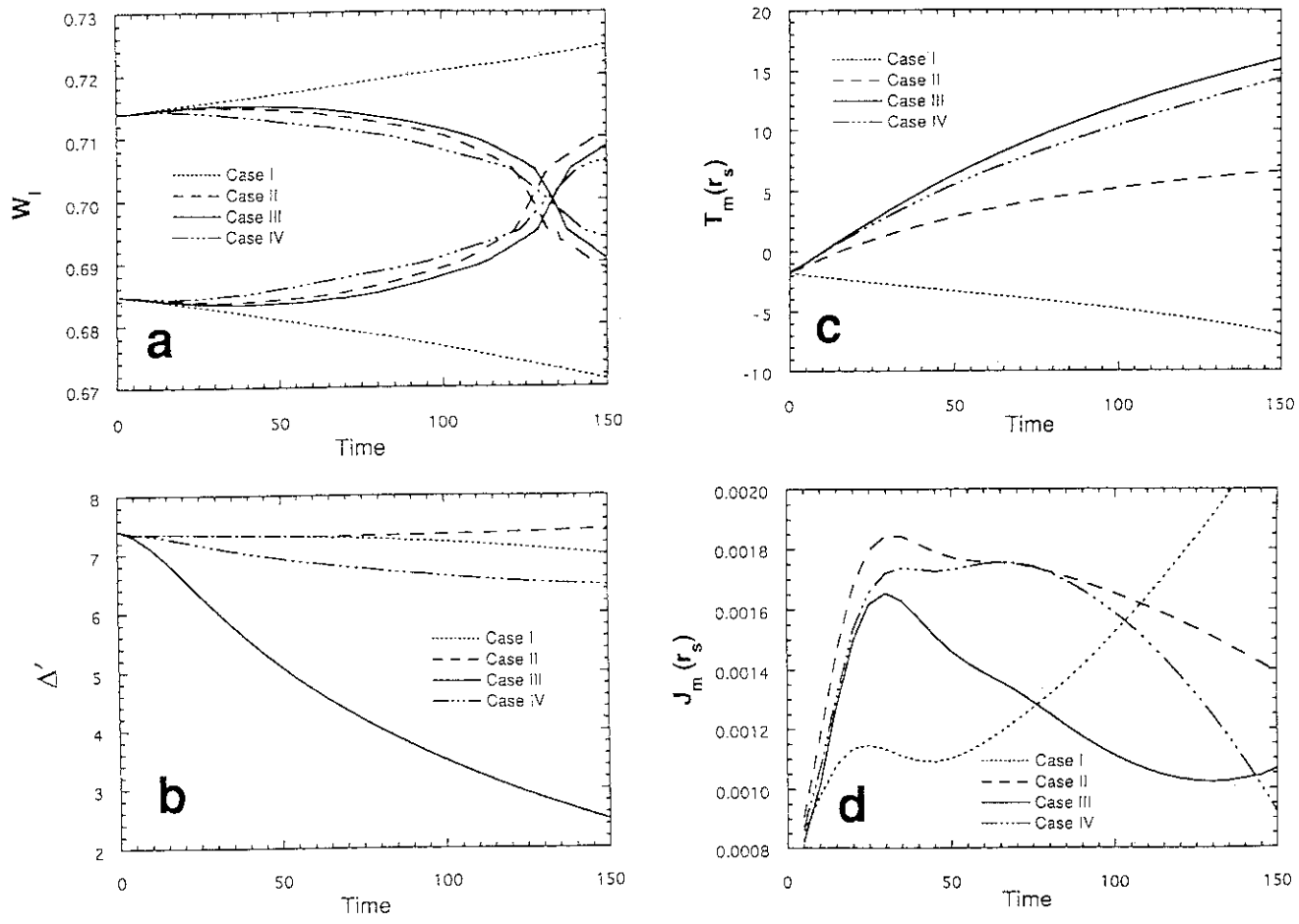

Fig. 2 Time evolutions of (a) width of magnetic island, (b) Δ', (c) electron temperature and (d) current density, where (c) and (d) are the amplitude of m=2 component at the singular surface of each function. Dotted, broken, solid and dotted solid curves correspond to the Cases I, II, III and IV, respectively.

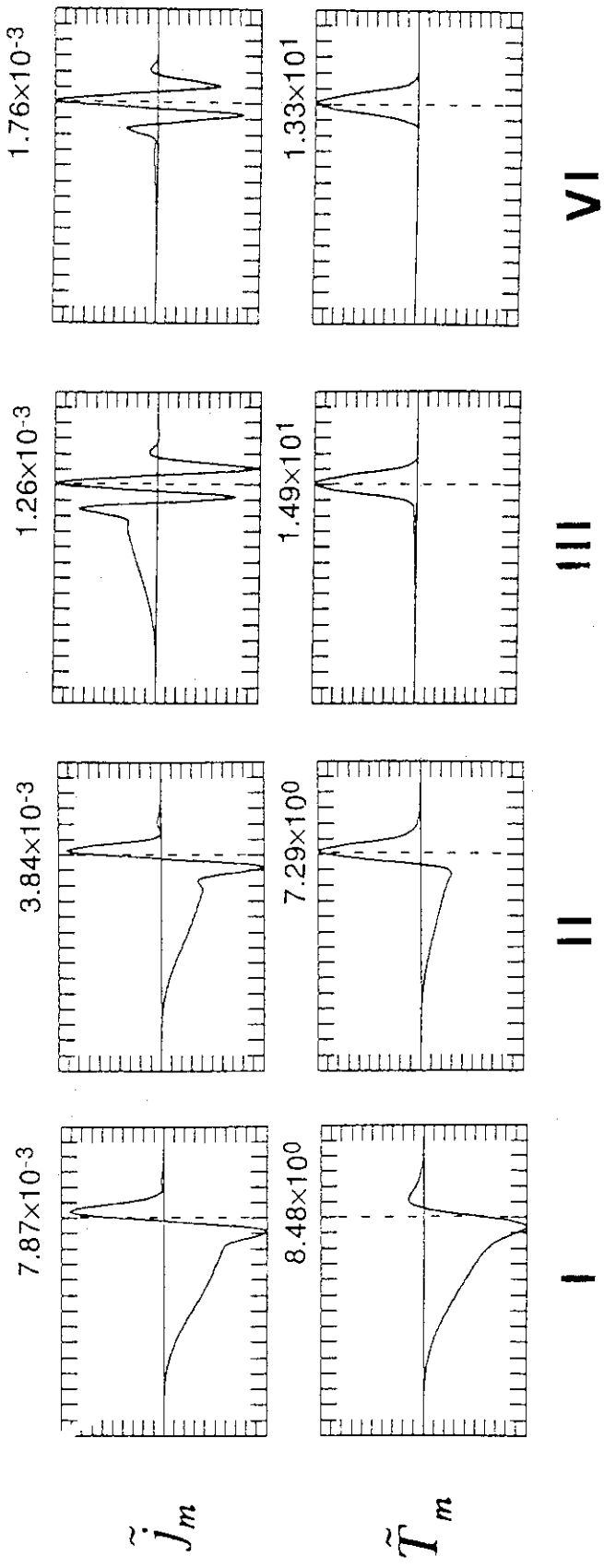

Fig. 3 Profiles of current density(upper subfigures) and electron temperature (lower subfigures) of m=2 component at t=130. Subfigures I, II, III and IV correspond to the Cases I, II, III and IV, respectively. Broken line in each subfigure denotes position of the singular surface, and each function is normalized to its absolute maximum value, which is shown on the upper side of each box.

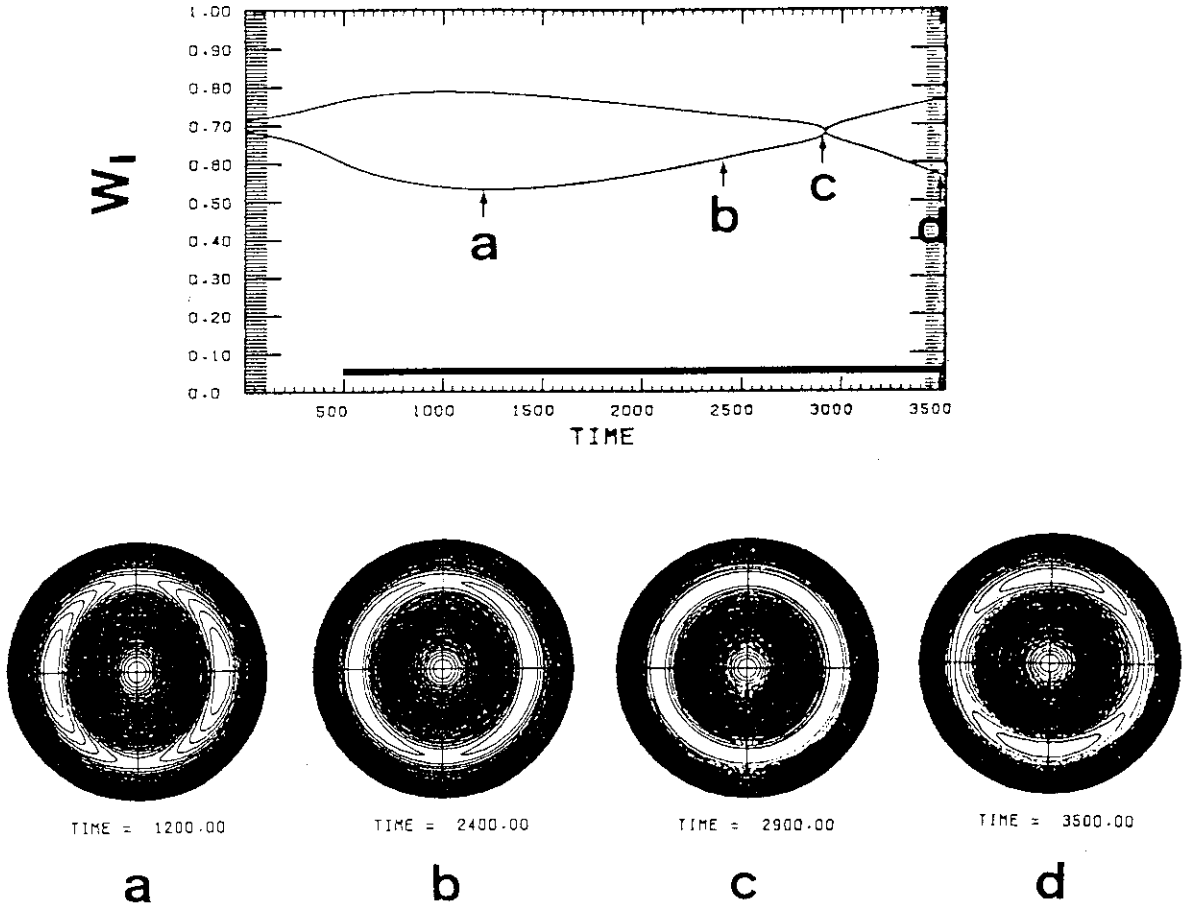

Fig. 4 Time evolutions of width of magnetic island using heat profile of Eq.(15) with $P_{rf}=10^{-4}$. The heat power is turned on at t=500, and the bold line denotes the duration of the heating. The lower subfigures are the contour of helical poloidal flux function at four points of time, denoted by arrows in the upper subfigure of magnetic island evolution.

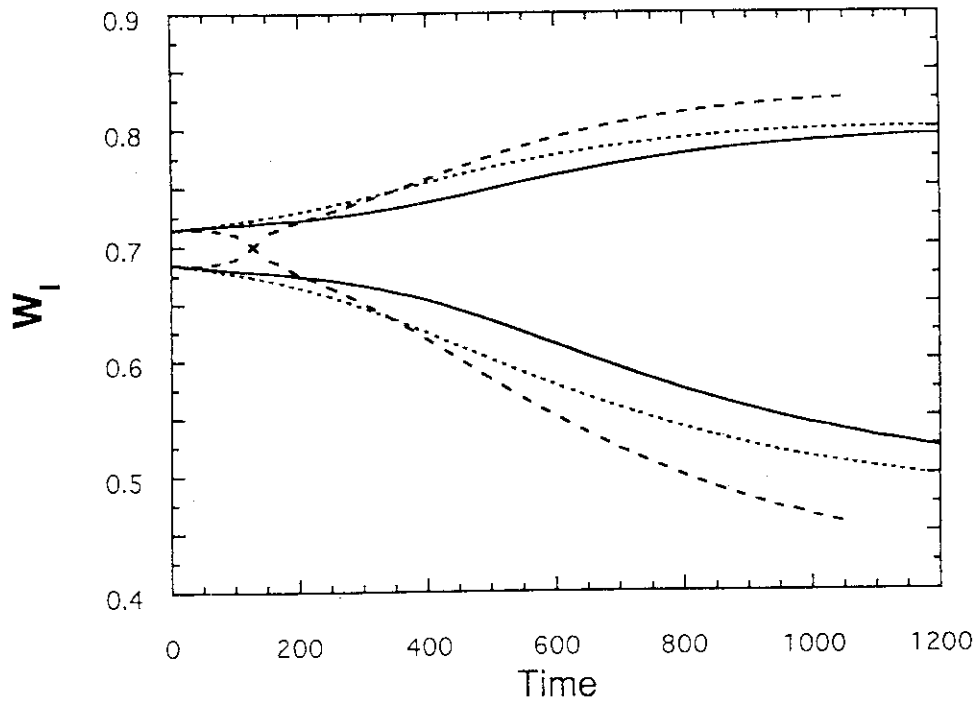

Fig. 5 Time evolutions of width of magnetic island for the heat profile of Eq.(15). Heat powers are $P_{rf}=10^{-4}$ for broken curves, $P_{rf}=3\times10^{-5}$ for solid curves and $P_{rf}=0$ (no heating) for dotted curves.

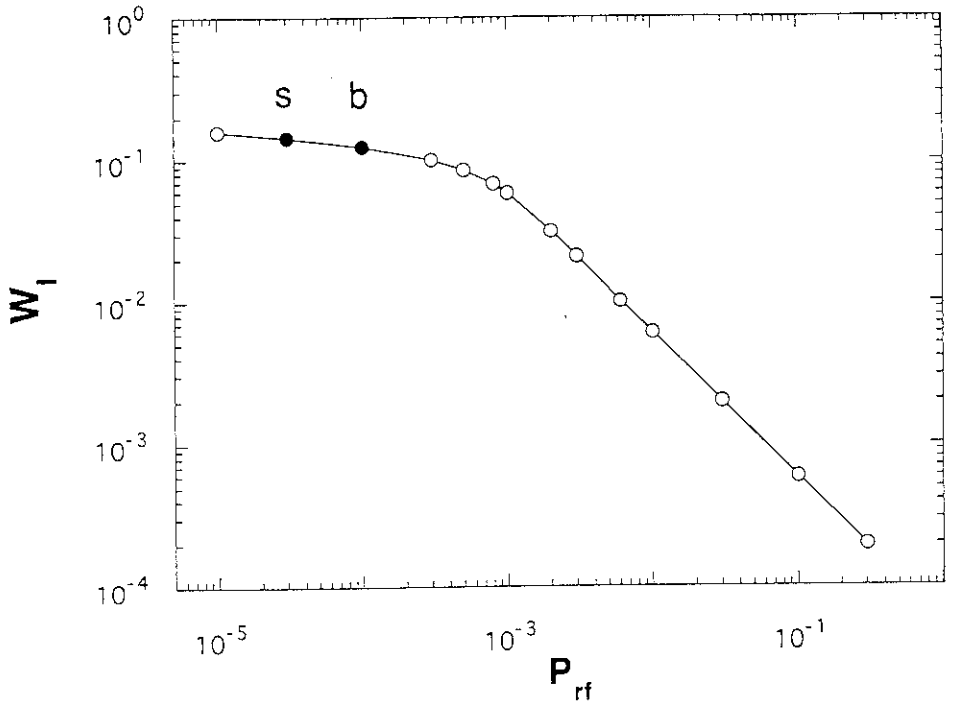

Fig. 6 Saturation width of magnetic island versus heat power obtained by solving Eq.(18). Two closed circles with the characters s and b correspond to the cases of simulations of solid and broken curves in Fig. 5, respectively.

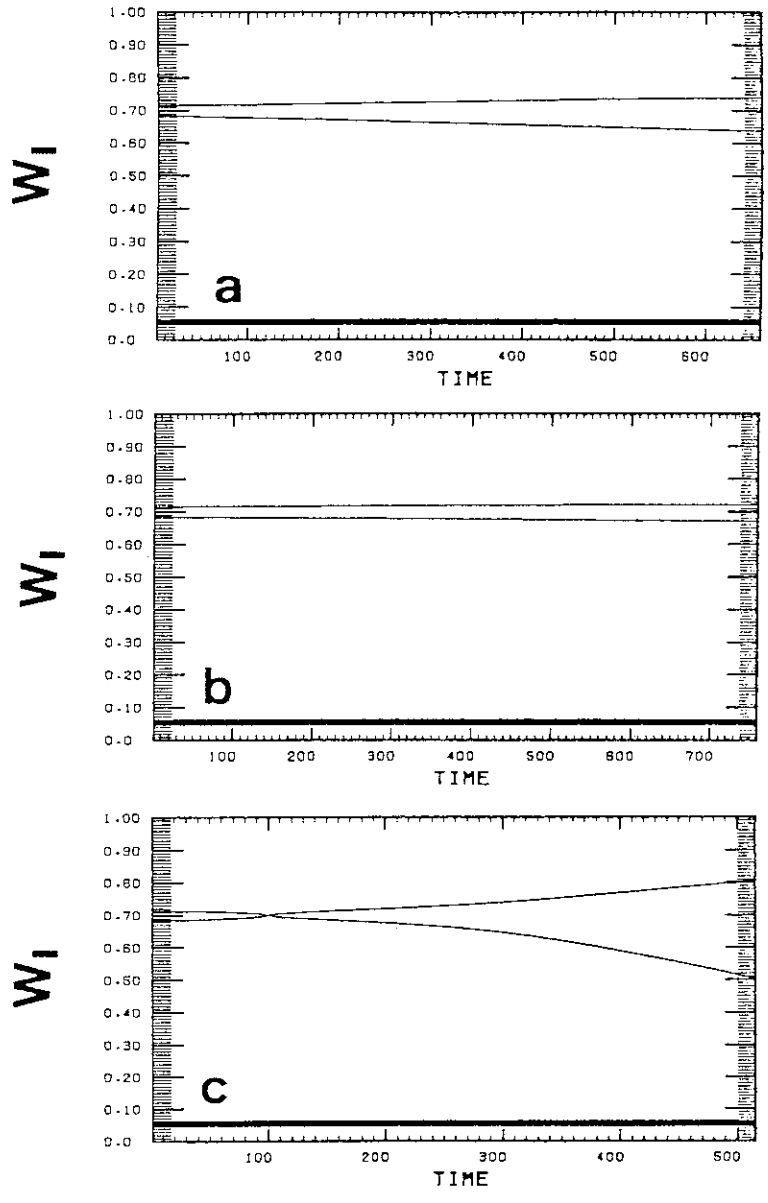

Fig. 7 Time evolutions of magnetic island width for large parallel conduction of electron temperature, $\kappa_{||}=10^{4}$. Heat power is (a) $P_{rf}=10^{-4}$, (b) $P_{rf}=3\times10^{-3}$ and (c) $P_{rf}=10^{-3}$. Other parameters are the same as in the case of Fig. 3.

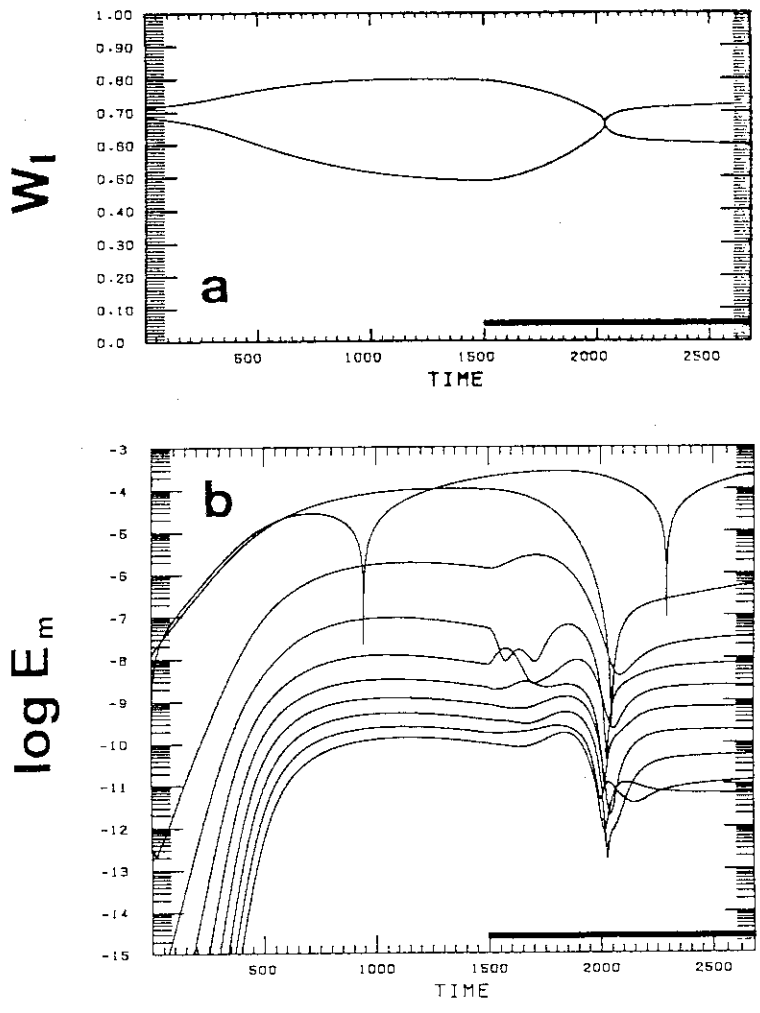

Fig. 8 Time evolutions of (a) width of magnetic island, and (b) magnetic energy of each mode. Heat power is turned on at t=1500, when magnetic islands are in saturation state. The heat parameters are $P_{rf}=5\times10^{-3}$ with $\delta_r=0.05$, $\delta_\theta=\pi/10$, $r_\delta(t)=r_s$ and $\theta_\delta=0$ in Eq.(12). The width of magnetic island becomes zero at t=2037, and magnetic island appears in opposite phase.

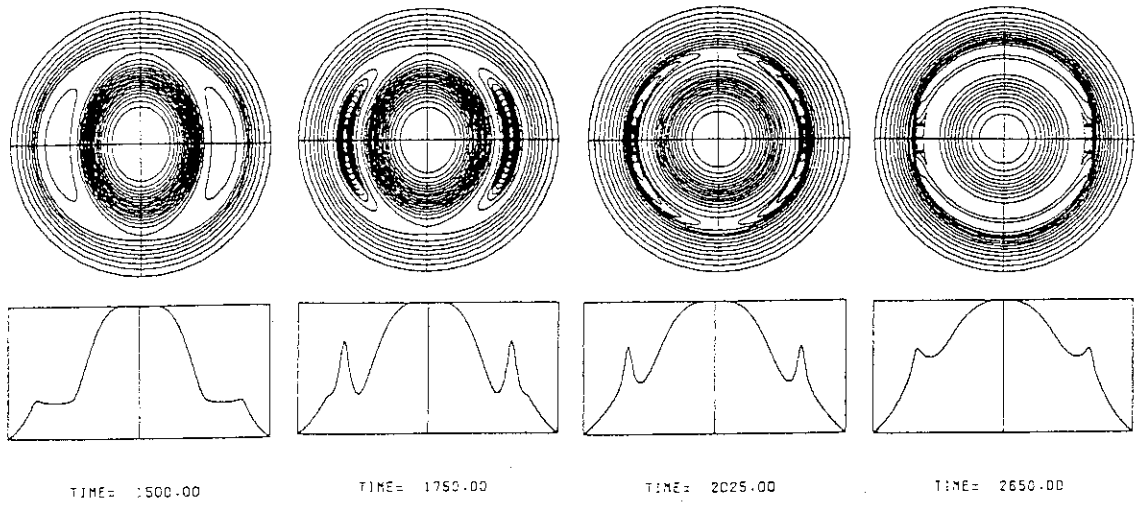

(a) electron temperature

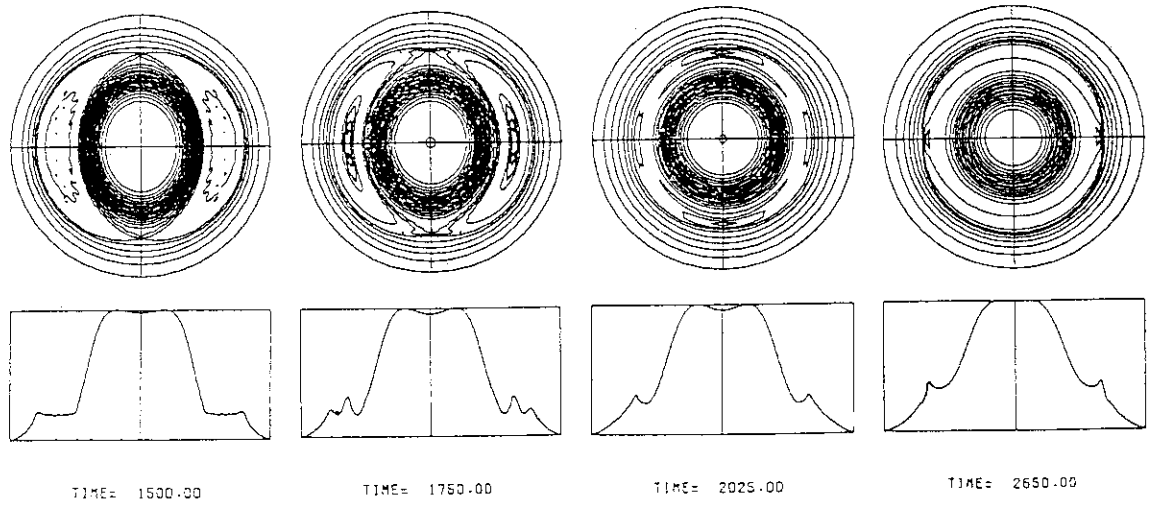

(b) current density

Fig. 9 Time evolutions of contours of (a) electron temperature and (b) current density at t=1500, t=1750, t=2025 and t=2650. The simulation parameters are the same as those of Fig. 8. Local positive perturbations of electron temperature induce positive local current perturbations.

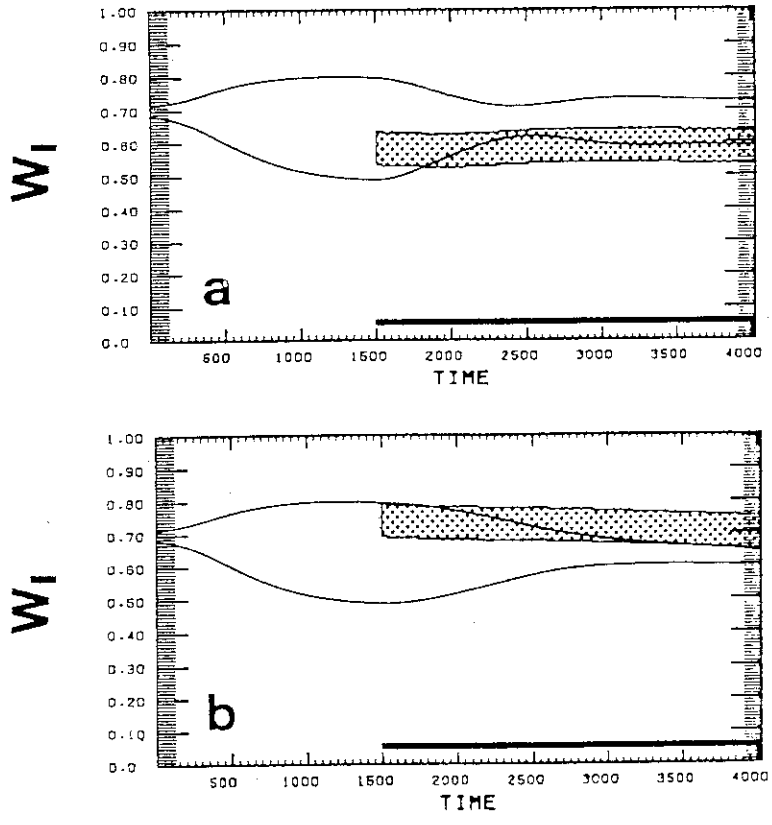

Fig. 10 Time evolutions of magnetic island for (a) δ_{rs}=−0.08 and (b) δ_{rs}=0.08. Radial heat regions are shown by dotted rectangles in each subfigure. Stabilizing effect ceases when the center of heat profile goes outside of the magnetic island.

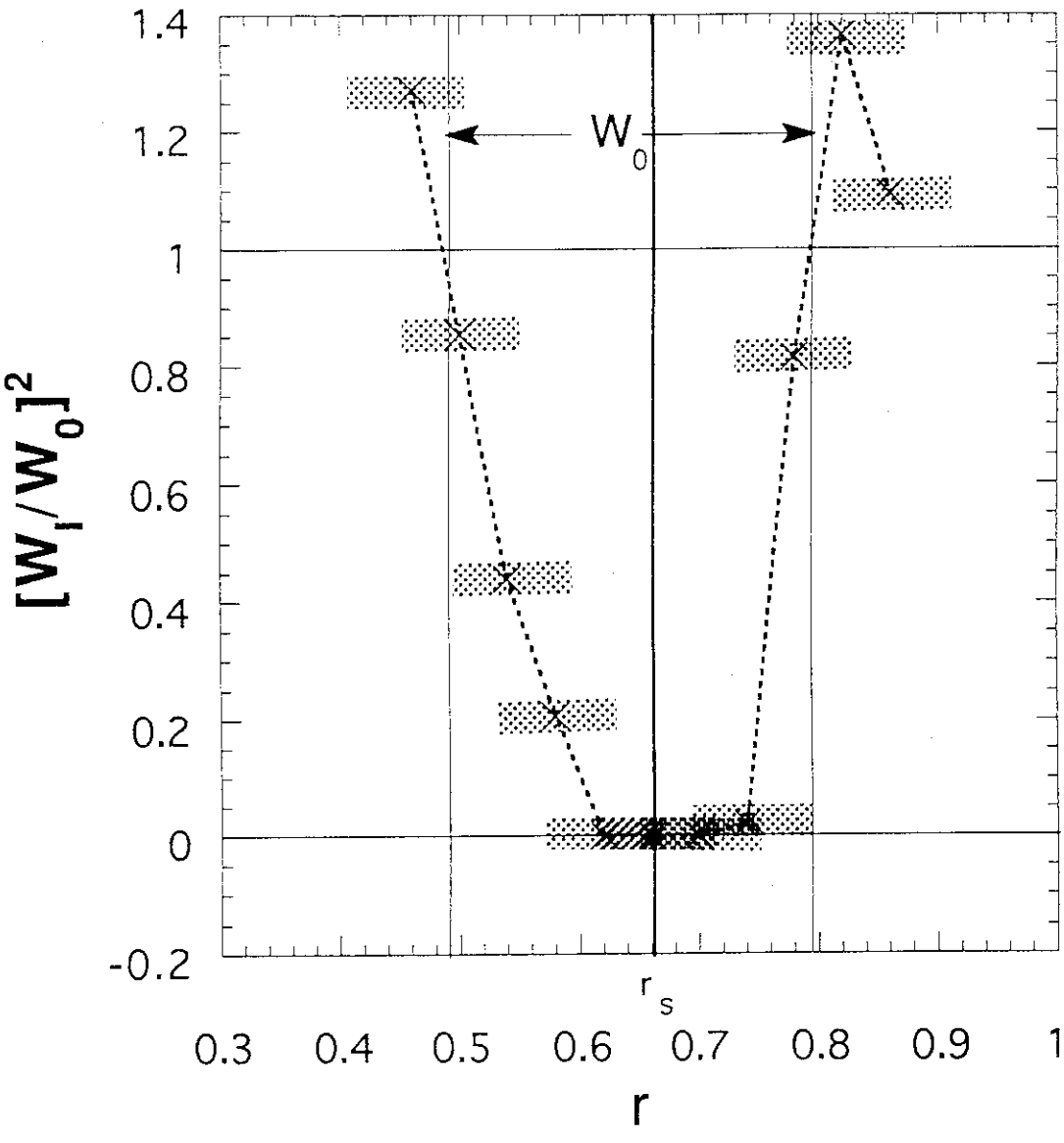

Fig. 11 Squared width of saturated magnetic island normalized to w_0, the saturation width without heat effect, versus radial position of heating. Dotted rectangles denote radial extent of heating.

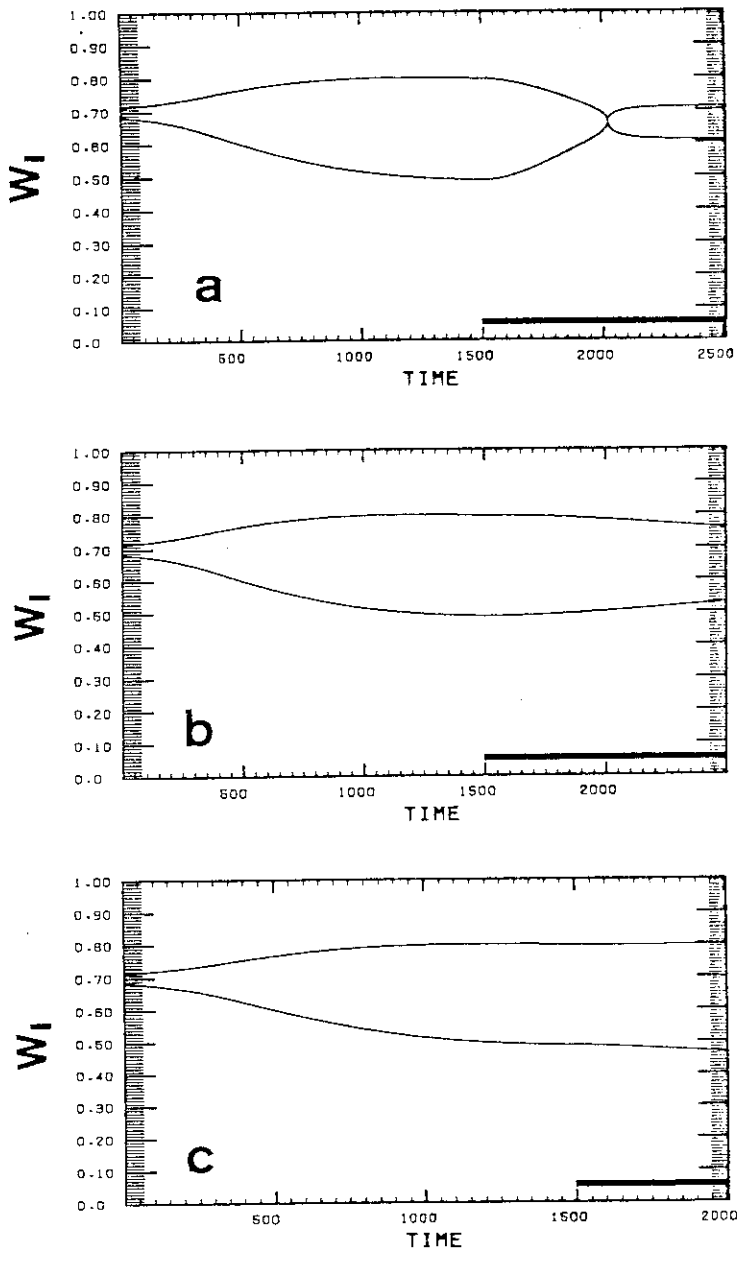

Fig. 12 Time evolutions of magnetic island width for different poloidal position of heating. Subfigures (a), (b) and (c) show the cases of $\theta_\delta=\pi/8$, $\theta_\delta=\pi/4$ and $\theta_\delta=\pi/2$, respectively. Other parameters are the same as in Fig. 8.

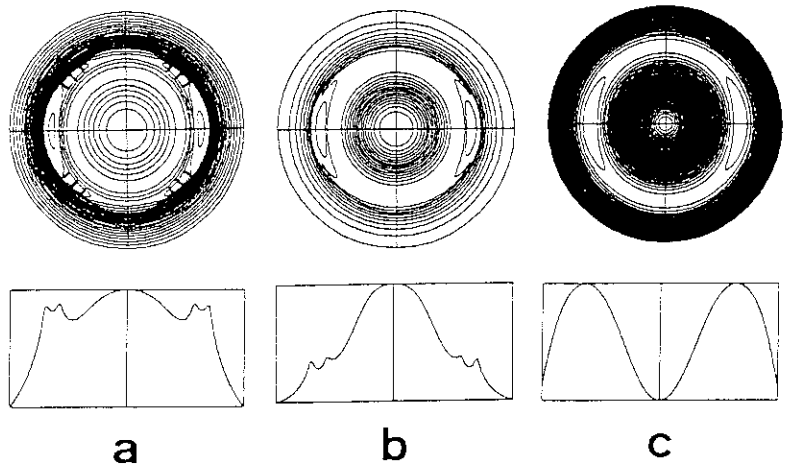

Fig. 13 Contour of (a) electron temperature, (b) current density and (c) helical poloidal flux function in the case of $\theta_\delta=\pi/4$(Fig. 12(b)). Four heat points appear because of symmetry assumed in basic equations.

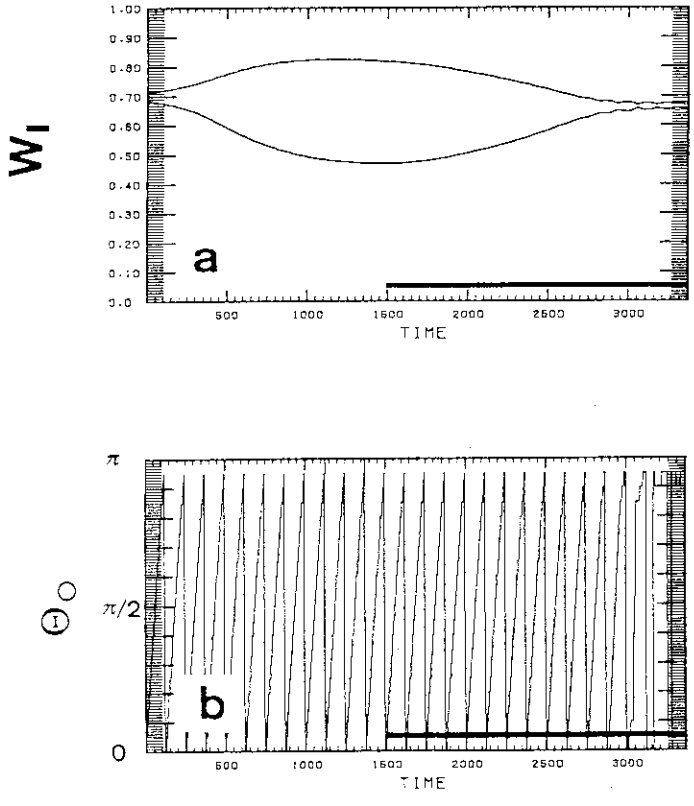

Fig. 14 Time evolutions of (a) rotating magnetic island width and (b) poloidal position of O-point of magnetic island. Plasma rotates as a rigid body with rotation period $\tau_S=250$ and heat power is turned on at t=1500.

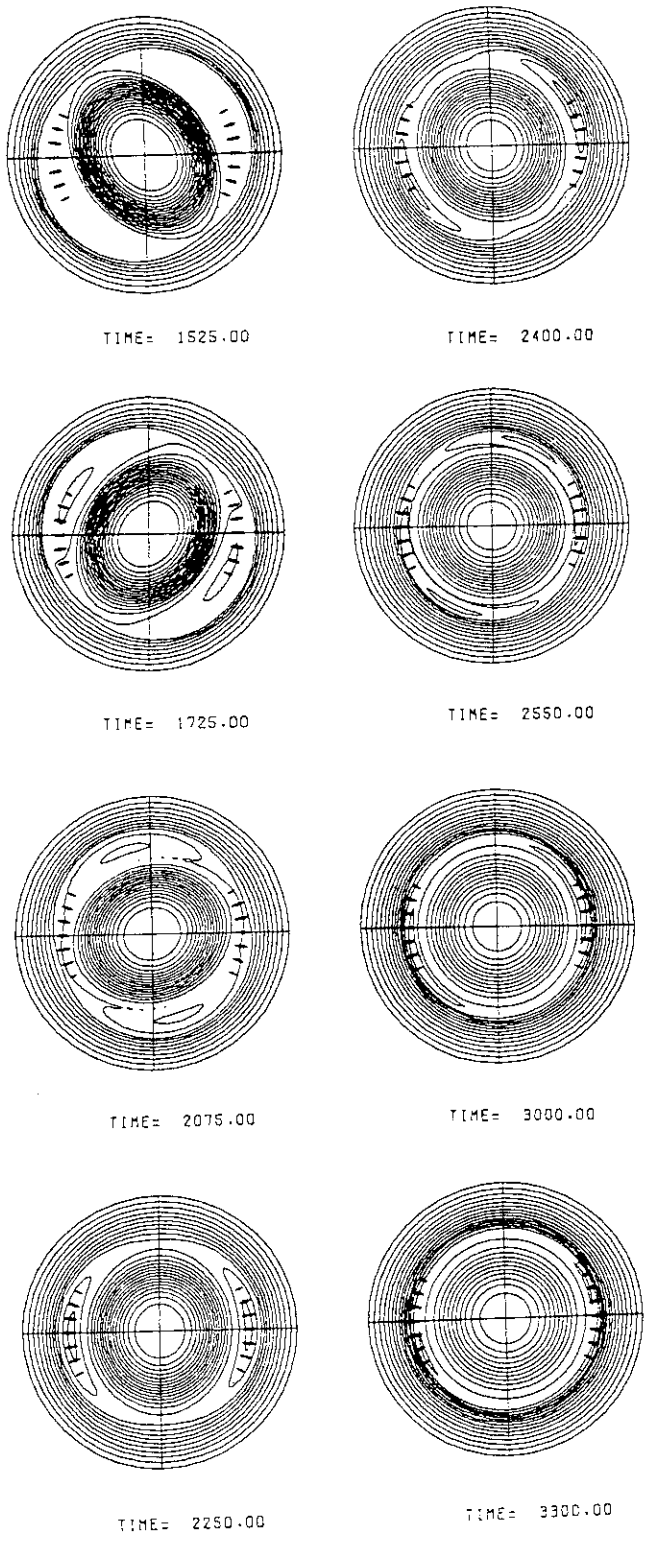

Fig. 15 Time evolutions of electron temperature contour at eight different time, which are shown below each subfigure, in the case of Fig. 14. Heat positions are denoted by bold solid lines on constant θ line.

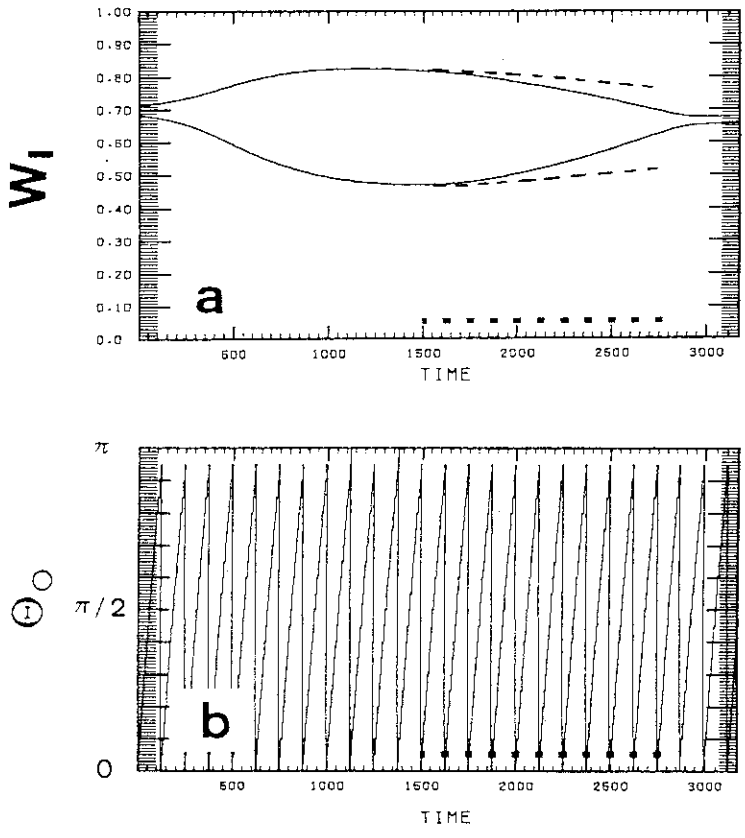

Fig. 16 Time evolutions of (a) width of rotating magnetic island and (b) O-point phase of magnetic island with feedback control of heat power. Solid curves show the case of O-point heating, while dotted curves are the case of X-point heating. The heat powers are supplied only when the poloidal position of magnetic island O-point is near $\theta=0$, as shown by bold dotted line. The poloidal positions of heating are at $\theta=0,\pi$ for O-point heating and $\theta=\pi/2$, $3\pi/2$ for X-point heating, respectively.